Thermoporometry study of coagulation bath temperature effect on polyacrylonitrile fibers morphology

Payman Sobhanipour [a,*], Reza Cheraghi [b], Alex A. Volinsky [c]

[a] Textile Engineering Department, Amirkabir University of Technology, Tehran 15914, Iran
[b] Textile Engineering Department, Isfahan University of Technology, Isfahan 84154-83111, Iran
[c] University of South Florida, Department of Mechanical Engineering, Tampa, FL 33620 USA

ABSTRACT

The effect of coagulation bath temperature on the morphology of wet-spun polyacrylonitrile fibers was investigated by scanning electron microscopy and thermoporometry, a calorimetric technique based on lowering liquid triple point temperature inside the pores. Fibers were fabricated at two coagulation bath temperatures of $5\,^\circ C$ and $60\,^\circ C$. The shape of nascent fibers cross-section transforms from bean to circular and pore size increases with coagulation temperature. Porosity parameters including average pore size and pore size distribution, pore volume and internal surface area were determined by thermoporometry. The average pore size and pore volume of the fibers increase with coagulation temperature. Low heating rate of $0.1\,^\circ C/min$ during thermoporometry measurements is the key parameter to ensure that test conditions are close to equilibrium. This study shows that thermoporometry can be employed to characterize closed meso-porosity of wet-spun fibers inaccessible by other standard porosimetry methods.

© 2011 Elsevier B.V. All rights reserved.

1. Introduction

Light weight carbon fibers (CFs) have outstanding mechanical properties (high tensile strength and elastic modulus), which makes them excellent engineering materials for aerospace, aviation and marine industries, and for use in high quality sporting goods [1–3]. Different precursors are employed to produce CFs, including polyacrylonitrile (PAN) fibers, viscose rayon, mesophase pitch. PAN fibers are most popular among carbon precursors because of their high carbon yield, economic processing and competitive pricing, high crystallinity, and continuous carbon backbone which facilitates the cyclization reaction [4–6]. It is clear that final CFs' properties strongly depend on the properties of PAN precursor fibers, i.e. orientation, crystallinity, linear density, shape of cross-section, porosity and co-monomer types [7–10].

PAN fibers are fabricated by different spinning methods like wet spinning, dry spinning and dry-jet-wet spinning. Meanwhile, wet spinning is the main fabrication method for PAN fibers employed by many researchers [6–10]. In this method polymer solution enters the coagulation bath after passing through the spinneret orifices. Here, non-solvent-induced phase separation (NIPS) is responsible for the fibers coagulation. Thermodynamic instability takes place in the polymer solution and separates it into polymer lean and

polymer rich phases. Polymer rich phase forms the fiber matrix which can solidify through different mechanisms, including gelation and/or crystallization. Polymer lean phase, which is full of solvent and non-solvent, forms the fiber pores. This kind of phase separation is called liquid–liquid de-mixing and is responsible for the appearance of porous structures [11]. Shape, size and distribution of the pores strongly depend on the exchange rate between the solvent and the non-solvent controlled by the process conditions, such as coagulation bath composition, temperature, and polymer solution additives [12].

Coagulation bath temperature has significant effects on the coagulation process by controlling the coagulation rate, i.e. exchange rate between solvent/non-solvent, and significantly affects physical properties of PAN fibers [13–15]. At low bath temperatures the rate of solvent out-diffusion is higher than the rate of non-solvent diffusing in. Consequently, fiber structure collapses and non-circular shapes including bean or dog bone cross-sections form. Also, slower coagulation results in less skin formation, leading to smaller and fewer voids.

According to the International Union of Pure and Applied Chemistry (IUPAC) recommendations, there are three pore size ranges, including micro-pores ($R < 2\,nm$), meso-pores ($2\,nm < R < 50\,nm$) and macro-pores ($R > 150\,nm$) [16]. For PAN fibers to be processed into CFs, the presence of meso-pores, macro-pores and especially closed pores significantly affects processing [17]. Therefore, sufficient knowledge of PAN precursor porosity is essential. There are several methods to determine pore size and pore size distribution of

the porous beds including sorption (1–100 nm), mercury porosimetry (1 nm to 10 μm), electron microscopy (10 nm to 1 μm), optical microscopy (1 μm), X-ray methods (0.1–100 nm) [18] and novel standard porosimetry method (0.3 nm to 300 μm) of Volfkovich et al. [19]. The numbers in parentheses show the pore size range detectable by each method. Each of these methods has advantages and limitations, but probing closed pores is still problematic.

Thermoporometry (TPM) is an alternative calorimetric method of meso-pores characterization based on lowering liquid triple point temperature inside the pores. When liquid is confined in meso-pores, its surface is no longer planar and has curvature. This configuration causes liquid to melt/freeze at temperatures lower than its normal transition temperature [20–25]. Brun et al. [26] derived a relationship between the temperature drop (ΔT) and pore radius (r_p) for melting of ice inside the pores from Gibbs–Duhem fundamental equation by considering the pores as cylinders with circular cross-section:

$$r_p = -\frac{32.33}{\Delta T} + 0.68 \quad \text{for} \quad 0 > \Delta T > -40\,^\circ\text{C} \tag{1}$$

where the value of 0.68 nm is the thickness of water layer that does not participate in any transition, named non-freezable water. It can be seen that ΔT inversely depends on r_p. This means that water transition temperature inside the pores gradually approaches its bulk temperature with increasing r_p. One can calculate other porosity parameters, including pore volume (V_p) and internal surface area (S_p) from the pore size distribution (PSD) curve, i.e. differential pore volume verses pore radius. In order to transform a thermograph of a differential scanning calorimeter (DSC) to PSD curve, Eq. (2) is employed [20]:

$$\frac{dV_p}{dr_p} = \frac{dQ}{dt}\frac{dt}{d(\Delta T)}\frac{d(\Delta T)}{dr_p}\frac{1}{m\Delta H_f(T)\rho(T)} \tag{2}$$

where dQ/dt is the heat flow, $dt/d(\Delta T)$ is the reverse of the heating rate, and m is the mass of a dry porous sample. Also, $\Delta H_f(T)$ and $\rho(T)$ are temperature-dependent heat of fusion and ice density, respectively. Parameter $d(\Delta T)/dr_p$ is derived from Eq. (1). $\Delta H_f(T)$ and $\rho(T)$ functions are described by Eqs. (3) [26] and (4) [20]:

$$\Delta H_f(T) = -0.155(T - T_0)^2 - 11.39(T - T_0)$$
$$-332 \quad \text{for} \quad 0 > \Delta T > -25\ ^\circ\text{C} \tag{3}$$

$$\rho(T) = 0.917(1.032 - 0.000117T) \tag{4}$$

There are a few studies dealing with applications of TPM method to determine PAN films and fibers porosity [27,28] and this paper investigated how TPM can be employed to characterize meso-porosity in the wet-spun PAN fibers.

In this paper, PAN fibers were spun in the system of water and dimethyl sulfoxide (DMSO) at two coagulation bath temperatures of 5 °C (PAN1) and 60 °C (PAN2) through wet spinning and their morphology was investigated by scanning electron microscopy (SEM) and TPM.

2. Experimental results

2.1. Materials

PAN copolymer (acrylonitrile:methyl acrylate:sodium 2-methyl-2 acrylamidopropane sulfonate = 94:5.6:0.4) in the form of powder was supplied by Polyacryl Co. (Isfahan, Iran) with the viscosity average molecular weight of 104,000 g/mol, which was obtained using an Ubbelohde viscometer and Mark-Houwink equation. The Mark–Houwink K and α parameters for N,N-dimethylformamide at 25 °C are 0.0243 ml/g and 0.75, respectively
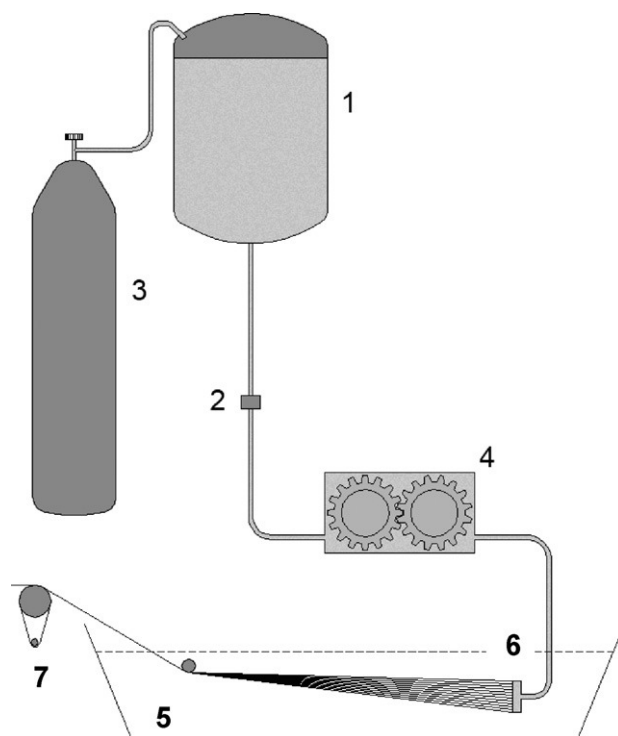

Fig. 1. Schematic of the laboratory wet spinning apparatus. Here, 1 is the dope vessel, 2 is the filter pack (10 μm filter mesh), 3 is nitrogen gas tank, 4 is fine gear pump that feeds the dope into the coagulation bath 5 through spinneret 6. (200 orifices, L/D = 1.2, 50 μm diameter). The nascent fibers are collected by the take-up roller 7 and washed with deionized water.

[29]. DMSO was purchased from Merck (Germany) and employed to dissolve PAN. Deionized water was used wherever necessary.

2.2. Wet spinning

Schematic of laboratory wet spinning apparatus is shown in Fig. 1. The PAN powder and DMSO are mixed in dope vessel (1) and stirred until a clear and homogenous polymer solution is prepared. Then the dope is driven to the filter pack (2) (10 μm filter mesh) by nitrogen gas (3). A fine gear pump (4) feeds the dope into the coagulation bath (5) through spinneret (6) (200 orifices, L/D = 1.2, 50 μm diameter). Finally, the nascent fibers are collected by take-up roller (7) and washed with enough deionized water for complete solvent extraction. Water inside the pores acts as the probe liquid responsible for the samples porosimetry according to the TPM method, thus the samples were kept in fresh deionized water to avoid water evaporation.

Two-step spinning process was performed. The following spinning parameters were used: 20% dope concentration (PAN %), 2.07 cm^2/min gear pump throughput, 65:35 DMSO:water bath concentration, 2.1 m/min take-up roller velocity, and 0.39 jet draw ratio. The main difference between the two processes is the coagulation bath temperature. PAN1 and PAN2 are the products of 5 °C and 60 °C bath temperatures, respectively. The apparent jet draw ratio was taken as the ratio of linear velocity of the take-up roller (V_2) to the linear velocity of the jet (V_1), i.e. V_2/V_1.

2.3. Thermoporometry

Differential scanning calorimeter (Mettler Toledo DSC823, Switzerland) was employed for thermal analysis, calibrated with deionized water. Nascent fibers were picked up from deionized water and cut carefully to 2 mm approximate length. TPM in melt-
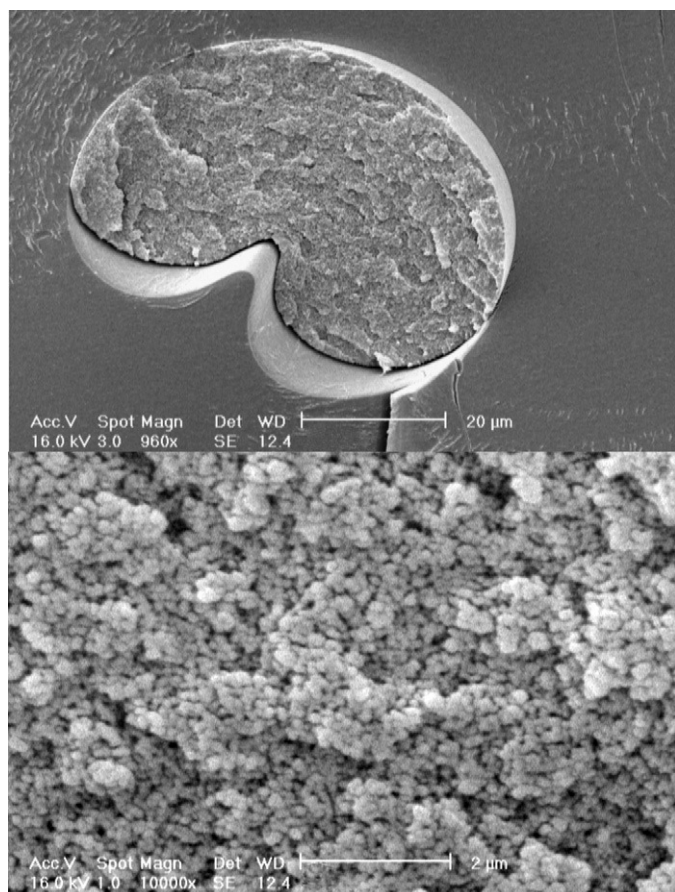
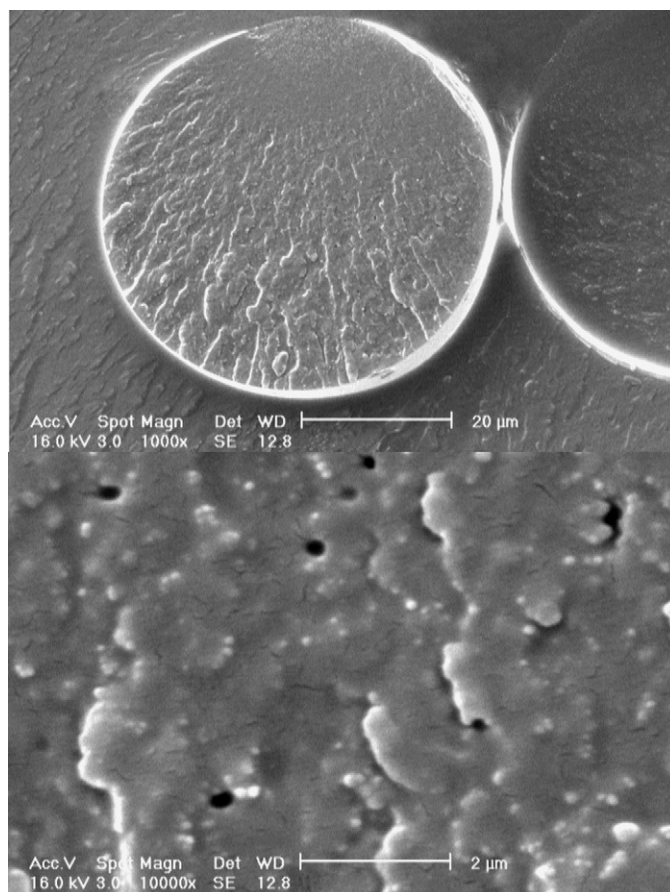**Fig. 2.** SEM images of wet-spun PAN1 (5 °C bath) fiber cross-section.

Fig. 3. SEM images of wet-spun PAN2 (60 °C bath) fiber cross-section.

ing mode was executed, i.e. the melting thermograph was recorded. About 2–5 mg of water-saturated wet-spun fibers were placed into DSC pan and immediately cooled to −60 °C, and held for 15 min at this temperature to ensure that water inside all pores froze. Heating was performed from −60 °C to 5 °C with 0.1 °C/min heating rate. These heating tests were repeated three times to evaluate reproducibility.

2.4. Scanning electron microscopy

The morphology of nascent fibers was investigated by SEM (Philips XL30). Samples were picked up from deionized water and dried at 70 °C in an oven for several hours. Then, a string of fibers was smeared with Epoxy resin mixed with hardener and left to be solidified in 50 °C oven for several hours. Finally, prepared composite was fractured in liquid nitrogen to produce smooth cross-sections.

3. Results and discussion

3.1. Morphology of nascent PAN fibers

SEM cross-sections of wet-spun PAN1 and PAN2 fibers are shown in Figs. 2 and 3, respectively. Clearly, cross-section shape changed from bean to circular when coagulation bath temperature increased, which is in good agreement with literature results [1,4,8,10]. This behavior is explained by the solvent and non-solvent counter-diffusion. During coagulation process there are two opposite flows, one is the diffusion of the non-solvent into the polymer solution (J_1) and the other is the diffusion of the solvent (J_2) out of the solution. When $J_1 \neq J_2$ the cross-section shape of the

coagulated fibers deviates from circular. This happens in the 5 °C coagulation bath. In this bath, $J_2 > J_1$, and the coagulating fibers are consequently collapsed and non-circular cross-section fibers are formed. The exact shape of the fibers cross-section also depends on the coagulation bath concentration. In this work the coagulation bath concentration was 65% DMSO. In the work of Ismail et al. [30] both cold and harsh water bath was employed to make dry-jet-wet-spun PAN fibers, which resulted in the dog bone cross-section shape. Since circular cross-section is the best for heat treatment in order to produce CFs, and PAN fibers have better properties at low coagulation temperatures, there are still many attempts to produce circular shape PAN fibers in cold coagulation baths.

The dominance of J_2 flow over J_1 in cold bath is better explained by the non-solvent molecules mobility. As a general idea, at lower temperatures the mobility of non-solvent molecules decreases, thus J_1 vector weakens and this condition consequently causes J_2 to take over J_1. Thus tension polarization on the surface is responsible for the fiber geometry. However, in warm bath, J_1 and J_2 vectors are in balance and there is no tension polarization. This explanation is convincing because of a good interaction between water and DMSO. These arguments are schematically demonstrated in Fig. 4.

By examining SEM images more carefully, it was found that the morphology of the wet-spun PAN fibers is free of macrovoids (MVs) for both PAN1 and PAN2. MVs are large cavities about 10–50 µm in diameter and their formation during coagulation process, especially in ternary systems, including non-solvent, solvent and polymer, is an undesirable phenomenon that weakens mechanical properties of membranes and fibers [12,31]. Rapid exchange of the non-solvent/solvent, i.e. fast precipitation facilitates the formation of MVs proposed by Kim et al. [32]. It is interesting to note that although coagulation rate increases with
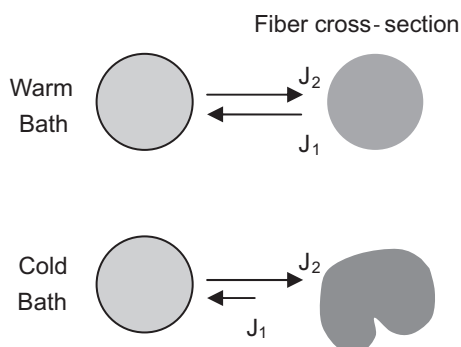
Fig. 4. Counter-diffusion of non-solvent/solvent in cold and warm baths.

bath temperature, there are no MVs in the wet-spun PAN2 fibers. Here high DMSO content of coagulation bath lowers the diffusion of non-solvent molecules into the coagulating fiber and balances J_1 and J_2 vectors.

Cross-section SEM images of wet-spun PAN1 and PAN2 fibers taken at higher magnification (Figs. 2b and 3b) show that the size and distribution of the pores are completely different for 5 °C and 60 °C baths. It is found that pore size increases with coagulation bath temperature, but pore distribution decreases. For PAN2 fibers there are sparse pores with the size of about 150–300 nm. However, for PAN1 fibers there is a widespread distribution of the pores with sizes between a few nanometers and 150 nm. This difference is explained by the coagulation mechanism, which is a complicated process, especially for fibers in wet spinning. Although not considered in this paper, rheological phenomena contribute to the morphology of wet-spun fibers in addition to kinetic and thermodynamic effects.

A tool to study phase behavior and coagulation mechanism of a ternary system is a phase diagram which shows non-solvent, solvent and polymer compositions at given pressure and temperature (Fig. 5). The phase diagram has three areas, including one phase area (I), meta-stable area (II) and two phase area (III). One phase and meta-stable areas are separated by binodal or liquid–liquid phase boundary. Also spinodal curve severs meta-stable and two phase areas from each other. The intercept of binodal and spinodal curves is called the critical point from which the phase separation starts. One can obtain binodal curve through titration of polymer solution by adding non-solvent (cloud point experiment) or calculating it through thermodynamic models of polymer solutions, e.g. Flory–Huggins model. Spinodal curve can only be calculated from thermodynamic models [12].
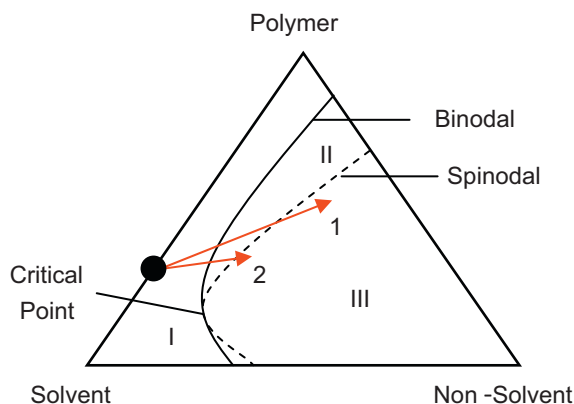

Fig. 5. Delayed de-mixing in the cold bath (vector 1) and instantaneous de-mixing in the warm bath (vector 2) during PAN fibers formation; non-solvent: water, solvent: dimethyl sulfoxide and polymer: polyacrylonitrile.
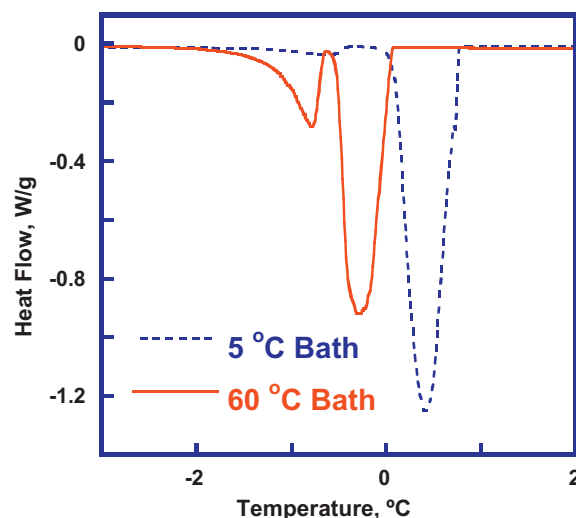

Fig. 6. DSC curves of water in warm and cold baths nascent fibers cooled to −60 °C and heated by 0.1 °C/min.

By induction of phase separation through the non-solvent addition (NIPS), thermodynamic instability occurs in the system and separates it into polymer rich phase (fiber matrix) and polymer lean phase (fiber pores). Polymer concentrations in initial solution (C_p) and at the critical point (C_c) determine the path through which coagulation occurs. When $C_p \neq C_c$ nucleation and growth (NG) of polymer rich phase ($C_p < C_c$) or NG of polymer lean phase ($C_p > C_c$) happens [33]. The NG mechanism is responsible for the formation of spherical pores (spongy structure). According to Dong et al. [2] studies of water/DMSO/PAN system phase behavior, the C_c value is about 5%. Since the C_p value in our system is 20%, NG of polymer lean phase undoubtedly happens. Spherical pore shape of the wet spun fibers (Figs. 2b and 3b) confirms the NG mechanism. However, the difference between size and distribution of the pores in the wet-spun fibers is still questionable.

When NG is dominant, the phase separation path goes through the meta-stable area demonstrated in Fig. 5 by vectors 1 and 2. In cold bath coagulation is slow or delayed, i.e. coagulation traverses a longer distance in the meta-stable area. This condition increases the nucleation density. Vector 1 in the phase diagram pertains to PAN1 phase separation path. Also, as discussed earlier, when $J_2 > J_1$, polymer concentration in the polymer rich phase gradually increases. This situation fixes the coagulating matrix and terminates pores growth. Vice versa in warm bath, phase separation path crosses the meta-stable area rapidly (instantaneous de-mixing). Then nuclei of the polymer lean phase have little time for growth and nucleation density is smaller than in the cold bath. However, due to the non-solvent penetration into the coagulating fibers, polymer lean phase can grow and the pore size increases. Vector 2 in Fig. 5 shows the coagulation path for PAN2.

3.2. Meso-porosity in nascent PAN fibers

DSC melting curves for water in nascent PAN fibers are displayed in Fig. 6. There are two endothermic peaks for each curve. The left peak pertains to melting of ice inside the meso-pores while the remaining ice outside of meso-pores melts at normal transition temperature of water recognized by the right peak. The peaks are completely apart, which confirms that heating was done close to equilibrium conditions. For PAN1 fibers, pore water had a weaker melting peak than for PAN2 fibers. Since the area of pore water peak pertains to V_p, it is expected that coagulated fibers in the warm bath have higher V_p than coagulated fibers in the cold bath.

Table 1
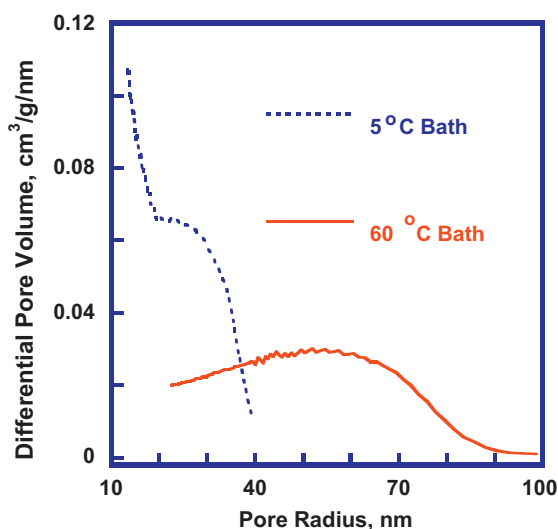Calorimetric data of pore water peaks and related pore sizes.

	PAN1, 5 °C bath	PAN2, 60 °C bath
Onset temp. (°C), pore size (nm)	−1.36 (19.05 nm)	−1.78 (22.52 nm)
Peak temp. (°C), pore size (nm)	−0.6 (33.01 nm)	−0.79 (66.66 nm)
Final temp. (°C), pore size (nm)	−0.43 (39.63 nm)	−0.63 (98.64 nm)

Water behavior in tiny nano-pores differs from the bulk. In fact, equilibrium temperature for a solid/liquid transition is determined by the radius of curvature of the interface between the solid and the liquid phases. In the bulk state water surface is planar and it melts/freezes at around 273.15 K. However, when water is confined in a nanometer pore, its surface is no longer planar and has curvature with high surface-to-volume ratio. Thus water phase transition temperature shifts below 273.15 K. It is important to note that the heating rate in a TPM experiment is the key parameter and should be set correctly. It means that the low heating rate is essential to keep the test conditions close to equilibrium. At high heating rates pore water and bulk water peaks approach each other and overlap, i.e. melting of ice in very small pores is not captured. This situation makes TPM calculations inaccurate and sometimes impossible. Arbab et al. [28] used the heating rate of 1 °C/min in their TPM porosimetry studies. The overlapped pore and bulk water endothermic peaks showed that this heating rate was chosen to some extent high. Also in the work of Price and Bashir [27], the heating rate of 4 °C/min seems to had the same problem. The effect of heating rate on TPM results was also discussed by Zeman et al. [34] and Landry [20].

Table 1 shows the onset, peak and final temperatures of pore water endothermic peaks for PAN1 and PAN2 fibers. Numbers in parentheses demonstrate the correlated pore size calculated using Eq. (1). To obtain ΔT, the peak temperature of the right bulk peak was considered to be 0.4 °C for PAN1 and −0.3 °C for PAN2. Therefore, the r_p for PAN1 is about 33 nm with 19–40 nm range. For PAN2 fibers, r_p is about 67 nm with 23–99 nm range. It is clear that r_p increases with coagulation bath temperature. Also PSD becomes better distributed with increasing coagulation bath temperature. The difference between the melting temperatures of bulk water arises from the fact that the weight ratio of water to dry porous sample affects the area and location of bulk water melting peak demonstrated by Landry [20]. In fact bulk water melting peak area increases and the peak shifts slightly to a higher temperatures as water to dry sample weight ratio increases. In the same way, pore water melting peak is moved to higher temperatures, therefore, temperature depression (ΔT) remains constant.

PSD curves for wet-spun PAN fibers are displayed in Fig. 7, calculated through equations (1)–(4). It is observed that although PAN1 have smaller pores than PAN2, their volume is higher, signified by a large peak area. This finding is in good agreement with SEM observations. From Figs. 2b and 3b, PAN1 fibers have smaller pores than PAN2 but the pores are distributed around the fiber cross-section. Therefore, it is expected for PAN1 fibers to have more internal surface area than for PAN2.

By comparing the results of TPM and SEM, it is found that pore size distribution of PAN1 is between 19 and 40 nm according to TPM method and changes from a few nanometers to 150 nm from SEM. Also, PAN2 showed a distribution of 23–99 nm via TPM technique and 150–300 nm according to SEM images. This comparison shows that the pore size distribution from two methods for each sample is a bit different; however, the trend, i.e. the increase in pore size with coagulation temperature is in agreement. This difference was expected because TPM only detects meso-pores (2–50 nm) while SEM visualizes both meso-pores and especially macro-pores. In other words, each method works in its respective size range.

Fig. 7. PSD curves of warm and cold baths wet-spun PAN fibers determined by TPM.

By integrating the PSD curves, V_p is determined to be 1.06 cm^3/g for PAN1 fibers and 1.46 cm^3/g for PAN2 fibers. By comparing the V_p values of PAN1 and PAN2 fibers, it is recognized that the pore volume values are close to each other as explained earlier. If it is assumed that the pores are true cylinders with circular cross-section, then internal surface area is calculated through $S_p = 2V_p/r_p$. Therefore, S_p for PAN1 is calculated at 64.24 m^2/g verses 43.77 m^2/g for PAN2 fibers. Since both fibers have approximately similar values of the pore volume and r_p for PAN2 fibers is about twice of PAN1, PAN1 have more internal surface area than PAN2.

4. Conclusions

In this work polyacrylonitrile (PAN) fibers were spun at two coagulation bath temperatures of 5 °C and 60 °C and the morphology of nascent fibers was investigated by scanning electron microscopy and calorimetric porosimetry method of thermoporometry. SEM images showed that by increasing the coagulation bath temperature, the shape of the fiber cross-section changes from bean to circular with larger pore size. These observations were explained by the counter-diffusion of non-solvent/solvent and by the phase behavior of water/PAN/DMSO system. Meso-porosity of PAN fibers was investigated through TPM and porosity parameters including average pore size (r_p), pore volume (V_p) and internal surface area (S_p) were calculated. Results showed that r_p and V_p increase with coagulation bath temperature. Wet-spun fibers at low coagulation temperature have higher surface area S_p than wet-spun fibers at high coagulation temperature.

This study also showed that TPM method can be employed to characterize meso-porosity of wet-spun PAN fibers which affects the properties of final carbon fibers. The main feature of the method is its ability to detect closed pores, inaccessible by other standard porosimetry methods.

References

[1] R. Dong, M. Keuser, X. Zeng, J. Zhao, Y. Zhang, C. Wu, D. Pan, Viscometric measurement of the thermodynamics of PAN terpolymer/DMSO/water system

and effect of fiber-forming conditions on the morphology of PAN precursor, J. Polym. Sci. B: Polym. Phys. 46 (19) (2008) 1997–2011.

[2] R. Dong, J. Zhao, Y. Zhang, D. Pan, Morphology control of polyacrylonitrile (PAN) fibers by phase separation technique, J. Polym. Sci. B: Polym. Phys. 47 (3) (2009) 261–275.

[3] X. Zeng, J. Hu, J. Zhao, Y. Zhang, D. Pan, Investigating the jet stretch in the wet spinning of PAN fiber, J. Appl. Polym. Sci. 106 (4) (2007) 2267–2273.

[4] P. Morgan, Carbon Fibers and Their Composites, Taylor & Francis, New York, 2005, pp. 121–148.

[5] Z. Wangxi, L. Jie, W. Gang, Evolution of structure and properties of PAN precursors during their conversion to carbon fibers, Carbon 41 (14) (2003) 2805–2812.

[6] J. Chen, C. Wang, H. Ge, Y. Bai, Effect of coagulation temperature on the properties of poly(acrylonitrile–itaconic acid) fibers in wet spinning, J. Polym. Res. 14 (3) (2007) 223–228.

[7] J.-J. Liu, H. Ge, C.-G. Wang, Modification of polyacrylonitrile precursors for carbon fiber via copolymerization of acrylonitrile with ammonium itaconate, J. Appl. Polym. Sci. 102 (3) (2006) 2175–2179.

[8] Y.-X. Wang, C.-G. Wang, M.-J. Yu, Effects of different coagulation conditions on polyacrylonitrile fibers wet spun in a system of dimethylsulphoxide and water, J. Appl. Polym. Sci. 104 (6) (2007) 3723–3729.

[9] J. Chen, H.-Y. Ge, X.-G. Dong, C.-G. Wang, The formation of polyacrylonitrile nascent fibers in wet-spinning process, J. Appl. Polym. Sci. 106 (1) (2007) 692–696.

[10] Y.-X. Wang, C.-G. Wang, Y.-J. Bai, Z. Bo, Effect of the drawing process on the wet spinning of polyacrylonitrile fibers in a system of dimethyl sulfoxide and water, J. Appl. Polym. Sci. 104 (2) (2007) 1026–1037.

[11] P.V.D. Witte, P.J. Dijkstra, J.W.A. Van Den Berg, J. Feijen, Phase separation processes in polymer solutions in relation to membrane formation, J. Membr. Sci. 117 (1996) 1–31.

[12] M. Mulder, Basic Principles of Membrane Technology, Kluwer Academic Publications, The Netherlands, 1991, pp. 123–134.

[13] P. Bajaj, T.V. Sreekumar, K. Sen, Structure development during dry–jet–wet spinning of acrylonitrile/vinyl acids and acrylonitrile/methyl acrylate copolymers, J. Appl. Polym. Sci. 86 (3) (2002) 773–787.

[14] S.H. Bahrami, P. Bajaj, K. Sen, Effect of coagulation conditions on properties of poly(acrylonitrile–carboxylic acid) fibers, J. Appl. Polym. Sci. 89 (7) (2002) 1825–1837.

[15] X.-G. Dong, C.-G. Wang, Y.-J. Bai, W.-W. Cao, Effect of DMSO/H$_2$O coagulation bath on the structure and property of polyacrylonitrile fibers during wet-spinning, J. Appl. Polym. Sci. 105 (3) (2007) 1221–1227.

[16] M.J.V. Bommel, A thermoporometry study of fumed silica/aerogel composites, J. Porous Mater. 4 (3) (1997) 143–150.

[17] L.A. Zlatoustova, V.N. Smirnova, V.A. Medvedev, A.T. Serkov, The macroporosity of polyacrylonitrile fibre, Fibre Chem. 34 (3) (2002) 200–202.

[18] J.-S. Tsai, The traps in characterisation of PAN and carbon fibers by the mercury porosimetry method, J. Polym. Res. 1 (4) (1994) 393–397.

[19] Y.M. Volfkovich, A.V. Sakars, A.A. Volinsky, Application of the standard porosimetry method for nanomaterials, Int. J. Nanotechnol. 2 (3) (2005) 292–302.

[20] M.R. Landry, Thermoporometry by differential scanning calorimetry: experimental considerations and applications, Thermochim. Acta 433 (1–2) (2005) 27–50.

[21] M. Wulff, Pore size determination by thermoporometry using acetonitrile, Thermochim. Acta 419 (1–2) (2004) 291–294.

[22] M. Iza, S. Woerly, C. Danumah, S. Kaliaguine, M. Bousmina, Simultaneous biaxial drawing of poly (ε-caprolactone) films, Polymer 41 (15) (2000) 5864–5885.

[23] T. Yamamoto, A. Endo, Y. Inagi, T. Ohmori, M. Nakaiwa, Evaluation of thermoporometry for characterization of mesoporous materials, J. Colloid Interface Sci. 284 (2) (2005) 614–620.

[24] T. Yamamoto, S.R. Mukai, K. Nitta, H. Tamon, A. Endo, T. Ohmori, M. Nakaiwa, Evaluation of porous structure of resorcinol–formaldehyde hydrogels by thermoporometry, Thermochim. Acta 439 (1–2) (2005) 74–79.

[25] I. Beurroies, R. Denoyel, P. Llewellyn, J. Rouquerol, A comparison between melting-solidification and capillary condensation hysteresis in mesoporous materials: application to the interpretation of thermoporometry data, Thermochim. Acta 421 (1–2) (2004) 11–18.

[26] M. Brun, A. Lallemand, J.-F. Quinson, C. Eyraud, A new method for the simultaneous determination of the size and shape of pores: the thermoporometry, Thermochim. Acta 21 (1) (1997) 59–88.

[27] D.M. Price, Z. Bashir, A study of the porosity of water-plasticised polyacrylonitrile films by thermal analysis and microscopy, Thermochim. Acta 249 (1995) 351–366.

[28] S. Arbab, N. Mohammadi, P. Noorpanah, Designing index of void structure and tensile properties in wet-spun polyacrylonitrile (PAN) fiber. I. Effect of dope polymer or nonsolvent concentration, J. Appl. Polym. Sci. 109 (6) (2008) 3461–3469.

[29] J. Brandrup, E.H. Immergut, E.A. Grulke, Polymer Handbook, vol. VII, 4th ed., Wiley, 1999, p. 11.

[30] A.F. Ismail, M.A. Rahman, A. Mustafa, T. Matsuura, The effect of processing conditions on a polyacrylonitrile fiber produced using a solvent-free free coagulation process, Mater. Sci. Eng. A 485 (1–2) (2007) 251–257.

[31] V.P. Khare, A.R. Greenberg, J. Zartman, W.B. Krantz, P. Todd, Macrovoid growth during polymer membrane casting, Desalination 145 (2002) 17–23.

[32] Y.D. Kim, J.Y. Kim, H.K. Lee, S.C. Kim, Formation of polyurethane membranes by immersion precipitation. II. Morphology formation, J. Appl. Polym. Sci. 74 (9) (1999) 2124–2132.

[33] Y.D. Kim, J.Y. Kim, H.K. Lee, S.C. Kim, Formation of polyurethane membranes by immersion precipitation. I. Liquid–liquid phase separation in a polyurethane/DMF/water system, J. Appl. Polym. Sci. 73 (12) (1999) 2377–2384.

[34] L. Zeman, G. Tkacik, P. Le Parloue, Characterization of porous sublayers in uf membranes by thermoporometry, J. Membr. Sci. 32 (2–3) (1987) 329–337.